Atomic Structure of (111) $SrTiO_3$/Pt Interfaces

Steffen Schmidt, Dmitri O. Klenov, Sean P. Keane, Jiwei Lu, Thomas E. Mates and Susanne Stemmer[a)]

Materials Department, University of California, Santa Barbara, CA 93106-5050

[a)]Corresponding author; Email: stemmer@mrl.ucsb.edu

Abstract

Atomic resolution high-angle annular dark-field imaging (HAADF) in scanning transmission electron microscopy was used to investigate the interface atomic structure of epitaxial, (111) oriented $SrTiO_3$ films on epitaxial Pt electrodes grown on (0001) sapphire. The cube-on-cube orientation relationship of $SrTiO_3$ on Pt was promoted by the use of a Ti adhesion layer underneath the Pt electrode. While a Ti-rich Pt surface was observed before $SrTiO_3$ growth, HAADF images showed an atomically abrupt $SrTiO_3$/Pt interface with no interfacial layers. The $SrTiO_3$ films contained two twin variants that were related by a 180° rotation about the $\langle 111 \rangle$ surface normal. HAADF images showed two different interface atomic arrangements for the two twins. The role of Ti in promoting (111) epitaxy and the implications for the dielectric properties are discussed.

Metal-perovskite-metal thin film heterostructures are the key elements of devices such as non-volatile ferroelectric memories [1], tunable microwave capacitors [2] or ferroelectric tunnel junctions [3]. Metal/ferroelectric interfaces control properties such as leakage currents [4], ferroelectric fatigue [5], tunnel barriers [3], and "interfacial deadlayers", i.e. an apparent thickness dependence of the polarizability of paraelectric perovskite thin films [6]. For many applications elemental metal electrodes such as Pt are preferred, because of their high electrical conductivities needed for high-frequency applications [7-9]. Despite their technological importance, relatively few studies have succeeded in obtaining an atomic level understanding of these interfaces. Pt/$SrTiO_3$ thin film heterostructures are an ideal model system [10-13]. $SrTiO_3$ is an incipient ferroelectric with the cubic perovskite structure and it has a small lattice mismatch with Pt (~ 0.4 % at room temperature). We have recently shown that (111) $SrTiO_3$ thin films can be grown epitaxially on (111) oriented epitaxial Pt electrodes on (0001) sapphire if a thin (~ 3 nm) Ti layer was deposited *under* the Pt electrode [13]. If no Ti layer was present, the $SrTiO_3$ thin films were predominantly (110) oriented, although they also showed an epitaxial relationship with the (111) Pt electrode [12]. Ti adhesion or surface layers have also been shown to promote epitaxial growth on (111) Pt grains for other perovskite films [14-17]. Although it is well-known that Ti diffuses through Pt electrodes [18-21], the precise mechanisms by which Ti underlayers control perovskite thin film textures are not fully understood. In the literature, it has been suggested that either a Pt-Ti intermetallic or TiO_2 on the Pt surface provide a templating layer for (111) epitaxial perovskite growth [14,17]. Furthermore, (111) oriented epitaxial $SrTiO_3$ thin films showed a much more pronounced thickness dependence of their permittivity than (110) oriented films [22]. This thickness

dependence is commonly modeled by an interfacial capacitance with a lower permittivity than the "bulk" of the film [6,23], but its origins are not understood. The goal of the present paper is therefore to determine the atomic structure of (111) $SrTiO_3$/Pt interfaces [11] with the ultimate objective of gaining an improved understanding of their role in controlling film orientation and dielectric properties.

200 nm thick Pt electrodes were deposited on basal plane sapphire substrates coated with a ~ 3 nm Ti layer using DC sputtering at a substrate temperature of 650 °C. The Ti layer was deposited by electron beam evaporation at room temperature. The surface root mean square roughness of the Pt electrodes was about 0.47 nm. The close-packed (111) Pt planes were aligned with the (0001) sapphire oxygen planes as described by $(111)_{Pt} \| (0001)_{Al_2O_3}$ and $[01\bar{1}]_{Pt} \| [10\bar{1}0]_{Al_2O_3}$. $SrTiO_3$ films of about 100±10 nm thickness were grown by radio-frequency magnetron sputtering from a stoichiometric target at about 700 °C in a Ar/O_2 gas mixture, using sputter conditions described elsewhere [24]. Interfaces were imaged along $\langle 110 \rangle$ and $\langle 112 \rangle$ by cross-section transmission electron microscopy (TEM). TEM samples were prepared by conventional methods with Ar ion milling as the final step. A field emission TEM operated at 300 kV (FEI Tecnai F30UT, C_S □ 0.52mm) was used for high-angle annular dark field (HAADF) imaging in scanning transmission electron microscopy (STEM) and conventional high resolution TEM (HRTEM). The detector inner semi angle for HAADF was 68 mrad. Secondary ion mass spectrometry (Physical Electronics 6650 Quadrupole SIMS) and x-ray photoelectron spectroscopy (Kratos Axis Ultra XPS) were used to analyze a Pt/Ti coated sapphire wafer without $SrTiO_3$. This wafer had been exposed to a 5 min "pre-sputtering" treatment in the $SrTiO_3$ growth chamber, which involved exposure to the sputter gases at the growth

temperature but with the shutters closed to prevent transport of the target species to the substrate. SIMS showed that Ti had diffused through the Pt electrode and that the surface was enriched with Ti. XPS showed that the surface Ti was oxidized, similar to what was observed by others [19,21]. X-ray diffraction (XRD) and selected area electron diffraction in TEM showed an epitaxial relationship between the $SrTiO_3$ film and the Pt electrode, as described by $(111)_{SrTiO_3} \| (111)_{Pt}$ and $[01\bar{1}]_{SrTiO_3} \| [01\bar{1}]_{Pt}$. Both the Pt electrode and the $SrTiO_3$ film contained two twin orientation variants, denoted "A" and "B", that were related by a 180° rotation about the $\langle 111 \rangle$ surface normal [12,13]. In $SrTiO_3$, the two twin variants differed in stacking along [111], i.e. AaBbCcAaBbCc vs. AcCbBaAcCbBa, where capital and small letters represent Sr-O or Ti layers, respectively. In the film interior twin boundaries were oriented mostly perpendicular to the film surface, but did not show pronounced faceting [13]. Films grew in an island (Volmer-Weber) growth mode, with threading dislocations accommodating small misorientations between the nuclei upon coalescence [13].

Figure 1 shows an HRTEM image of the interface between Pt and one of the $SrTiO_3$ twin variants. The interface appeared atomically abrupt. The inset in Fig. 1 shows an atomic resolution HAADF/STEM image of a twin boundary. HAADF images are not subject to contrast reversals [25], and interface atomic arrangements of cations can be directly inferred. The contrast in HAADF reflects atomic number (*Z*) differences [25]. Bright features corresponded to Sr-O columns and weaker features to the Ti columns. Oxygen-only columns were not visible in these images. The overlay shows the atomic arrangement observed in this portion of the twin boundary, which corresponded to a

symmetrical $\Sigma 3(\bar{1}12)[110]$ twin; however, other atomic configurations were also observed [13]. The spacings between adjacent (111) planes measured across the boundary were larger than expected from a simple coincidence site lattice model of the boundary and adjacent Ti columns were significantly shifted along the film normal.

Figure 2 shows atomic resolution HAADF/STEM images of the interface between the two $SrTiO_3$ twin variants and one of the Pt variants. Due to the strong *Z*-contrast of this technique, Pt ($Z = 78$) was extremely bright. To show the atomic arrangement of both $SrTiO_3$ and Pt across the interface in one image, the brightness/contrast settings were adjusted differently in the upper and lower portions of the images, which is the origin of the artificial sharp line below the terminating Pt layer. In bulk $SrTiO_3$, SrO_3^{4-} planes alternate with Ti^{4+} layers along $\langle 111 \rangle$. No crystallographically distinct interface phase, i.e. with an atomic arrangement not found in either bulk Pt or $SrTiO_3$, could be observed in these images.

Both twins showed identical lattice translations parallel to the interface within an error of about 0.16 Å when imaged along $\langle 110 \rangle$ (corrections were made for image distortions typical for STEM by calibrating the spacings in the bulk of the films to bulk lattice parameters). In contrast, the two twins differed in their atomic arrangement in the direction normal to the interface. Quantified in terms of the distance between the first clearly identifiable Sr-O plane and the last Pt plane, the separation was 0.33±0.04 nm for twin A [Fig. 2(a)], whereas in twin B [Fig. 2(b)] it was 0.25±0.04 nm (see horizontal lines in Fig. 2). The distance between the terminating Pt and first Ti plane in twin A was 0.2±0.02 nm. The difference in the stacking normal to the interface for the two twin

variants was confirmed using several images and resulted in a relative shift of the two twins parallel to the twin boundary, which was found to relax through the film thickness.

The terminating $SrTiO_3$ plane of twin B was clearly a Sr-O plane. In twin A, the last clearly visible plane near the interface was a Ti plane (see Fig. 2), but it was possible that a partially occupied Sr-O plane was present very close to the Pt as some contrast that could correspond to Sr columns was occasionally observed. The difficulty in detecting Sr (or any other light atom) very near the last Pt layer stems from the large difference in background intensity between the heavy Pt electrode and the lighter $SrTiO_3$ film, as pointed out elsewhere [26]. This caused the background intensity at the interface plane to be intermediate between that of Pt and in $SrTiO_3$, potentially obscuring lighter atoms if they were present very close to the terminating Pt plane. Intensity line profiles showed that last Pt layer was likely fully occupied, despite a somewhat reduced total intensity (Fig. 2), because the intensity *above* the background in this layer was almost identical to that in bulk Pt.

Density-functional calculations of very thin Pt layers on (111) $SrTiO_3$ showed almost no difference in the energetics between the two terminations [10], but these calculations did not take different $SrTiO_3$ stacking into account. If interatomic forces acted beyond nearest neighbors, then the two twins were not energetically equivalent, as they differ in their stacking sequences. In this case at least part of that energy difference could have been mediated by the different interface atomic arrangement.

With respect to the role of Ti in promoting epitaxial (111) growth, the images did not show any evidence for templating by either an interfacial TiO_2 or a Pt-Ti intermetallic layer. While Ti-O surface layers observed in XPS could have been either not continuous or

consumed by the growing $SrTiO_3$ film, it was also possible that the effect of Ti in promoting (111) $SrTiO_3$ film epitaxy was more complex than simply providing a templating layer for (111) perovskite growth. For example, Ti may also play a role in gettering impurities from the growth surface [27]. Generally the orientation dependence of the energy of small nuclei was likely complicated for films that grew in a Volmer-Weber growth mode. Furthermore, the thickness dependent dielectric permittivity [22] could not be explained with the presence of any chemically distinct interface phase at the bottom electrode interface. The use of Ti adhesion layers was thus not expected to degrade the interfacial electric or dielectric properties of the capacitors. Possible alternative explanations for the pronounced thickness dependence of the permittivity include strain gradients through the film. This is consistent with our earlier studies that showed a greater extended defect density near the bottom interface [13] and studies by others that showed that thin, unclamped barium titanate single crystals exhibited bulk dielectric properties [28].

The authors gratefully acknowledge support for this research by the DOE Office of Basic Energy Sciences under grant #DE-FG03-02ER45994. S.P.K. thanks the National Science Foundation IGERT program (Award No. DGE-9987618) for support. This work made use of MRL Central Facilities supported by the MRSEC Program of the National Science Foundation under award No. DMR 05-20415.

References

1. O. Auciello, J. F. Scott, and R. Ramesh, Physics Today **July,** 22 (1998).
2. A. K. Tagantsev, V. O. Sherman, K. F. Astafiev, J. Venkatesh, and N. Setter, J. Electroceram. **11,** 5 (2003).
3. M. Y. Zhuravlev, R. F. Sabirianov, S. S. Jaswal, and E. Y. Tsymbal, Phys. Rev. Lett. **94,** 246802 (2005).
4. G. W. Dietz, M. Schumacher, R. Waser, S. K. Streiffer, C. Basceri, and A. I. Kingon, J. Appl. Phys. **82,** 2359 (1997).
5. H. N. Al-Shareef, K. R. Bellur, A. I. Kingon, and O. Auciello, Appl. Phys. Lett. **66,** 239 (1995).
6. C. Zhou and D. M. Newns, J. Appl. Phys. **82,** 3081 (1997).
7. J. D. Baniecki, R. B. Laibowitz, T. M. Shaw, P. R. Duncombe, D. A. Neumayer, D. E. Kotecki, H. Shen, and Q. Y. Ma, Appl. Phys. Lett. **72,** 498 (1998).
8. K. Ikuta, Y. Umeda, and Y. Ishii, Jpn. J. Appl. Phys. Part 2 **34,** L1211 (1995).
9. D. C. Dube, J. Baborowski, P. Muralt, and N. Setter, Appl. Phys. Lett. **74,** 3546 (1999).
10. A. Asthagiri and D. S. Sholl, Surf. Sci. **581,** 66 (2005).
11. A. D. Polli, T. Wagner, T. Gemming, and M. Rühle, Surf. Sci. **448,** 279 (2000).
12. S. Schmidt, J. W. Lu, S. P. Keane, L. D. Bregante, D. O. Klenov, and S. Stemmer, J. Amer. Ceram. Soc. **88,** 789 (2005).
13. S. Schmidt, Y.-W. Ok, D. O. Klenov, J. W. Lu, S. P. Keane, and S. Stemmer, J. Mater. Res. **20,** 2261 (2005).
14. T. Tani, Z. Xu, and D. A. Payne, Mat. Res. Soc. Symp. Proc. **310,** 269 (1993).

15. K. Aoki, Y. Fukuda, K. Numata, and A. Nishimura, Jpn. J. Appl. Phys. Part 1 **34,** 192 (1995).

16. C. S. Hwang, M. D. Vaudin, and P. K. Schenck, J. Mater. Res. **13,** 368 (1998).

17. P. Muralt, T. Maeder, L. Sagalowicz, S. Hiboux, S. Scalese, D. Naumovic, R. G. Agostino, N. Xanthopoulos, H. J. Mathieu, L. Patthey, and E. L. Bullock, J. Appl. Phys. **83,** 3835 (1998).

18. T. C. Tisone and J. Drobek, J. Vac. Sci. Technol. **9,** 271 (1971).

19. G. R. Fox, S. Trolier-McKinstry, S. B. Krupanidhi, and L. M. Casas, J. Mater. Res. **10,** 1508 (1995).

20. M. DiBattista and J. W. Schwenk, J. Appl. Phys. **86,** 4902 (1999).

21. K. Sreenivas, I. Reaney, T. Maeder, N. Setter, C. Jagadish, and R. G. Elliman, J. Appl. Phys. **75,** 232 (1994).

22. S. P. Keane, S. Schmidt, J. W. Lu, and S. Stemmer, Accepted for publication in: J. Appl. Phys. (Feb. 15, 2006 issue).

23. C. Basceri, S. K. Streiffer, A. I. Kingon, and R. Waser, J. Appl. Phys. **82,** 2497 (1997).

24. J. W. Lu, S. Schmidt, Y.-W. Ok, S. P. Keane, and S. Stemmer, J. Appl. Phys. **98,** 054101 (2005).

25. P. D. Nellist and S. J. Pennycook, Adv. Imaging Electron Physics **113,** 147 (2000).

26. D. O. Klenov, J. M. Zide, J. D. Zimmerman, A. C. Gossard, and S. Stemmer, Appl. Phys. Lett. **86,** 241901 (2005).

27. A. G. Evans, J. W. Hutchinson, and Y. Wei, Acta Mater. **47,** 4093 (1999).

28. M. M. Saad, P. Baxter, R. M. Bowman, J. M. Gregg, F. D. Morrison, and J. F. Scott, J. Phys.-Cond. Matter **16,** L451 (2004).

Figure Captions

Figure 1 (color online)

HRTEM of the Pt/STO interface recorded along $\langle 110 \rangle$. The inset shows an HAADF/STEM image of a symmetrical $\Sigma 3(\bar{1}12)[110]$ STO twin viewed along $\langle 110 \rangle$. The overlay shows the atom positions in the interface plane (the oxygen-only columns were not visible and their positions were inferred from the cation positions). Note the vertical displacements of closely spaced Ti columns.

Figure 2 (color online)

HAADF/STEM images of the interface between $SrTiO_3$ and Pt for (a) twin variant A and (b) twin variant B recorded along the $\langle 110 \rangle$. Red and green horizontal lines mark the position of Sr-O (111) layers and Pt (111) planes, respectively. The overlay shows the average atom column positions (see legend in Fig. 1) determined from intensity line scans across several locations in the images. The oxygen-only columns were not visible and their positions were inferred from the cation positions.

Figure 1

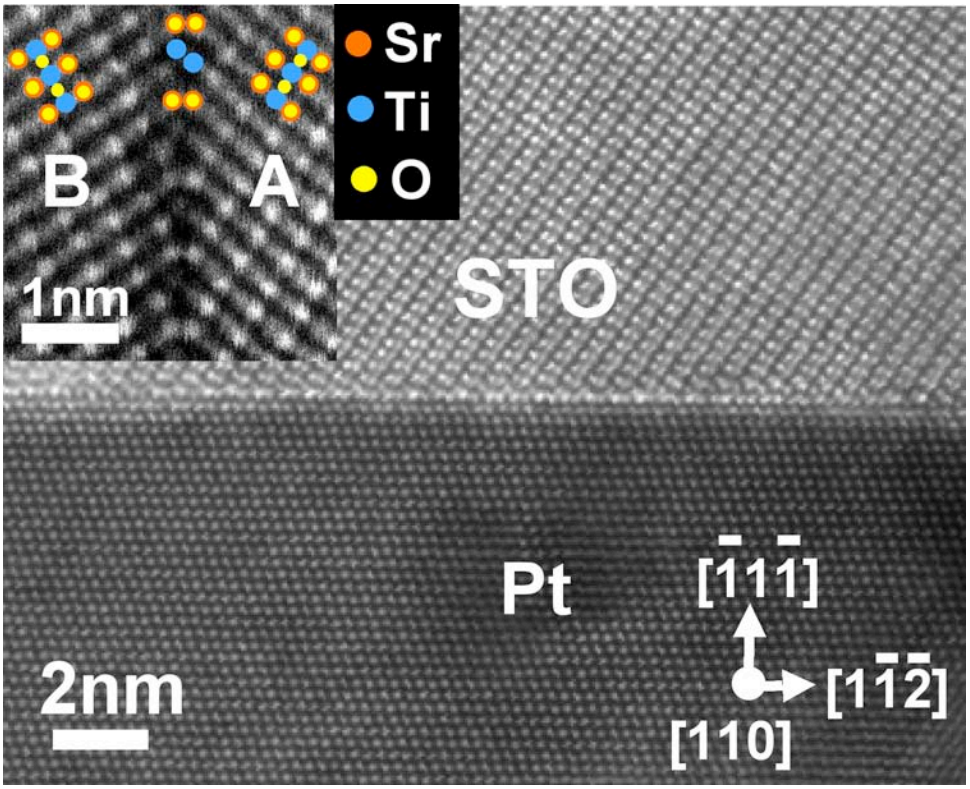

Figure 2